A multibody kinematic system approach for the design of shape-morphing mechanism-based metamaterials

de Jong, Pier H.; Schwab, A. L.; Mirzaali, Mohammad J.; Zadpoor, Amir A.

DOI
10.1038/s43246-023-00410-2

Publication date
2023

Document Version
Final published version

Published in
Communications Materials

Citation (APA)
de Jong, P. H., Schwab, A. L., Mirzaali, M. J., & Zadpoor, A. A. (2023). A multibody kinematic system approach for the design of shape-morphing mechanism-based metamaterials. *Communications Materials*, *4*(1), Article 83. https://doi.org/10.1038/s43246-023-00410-2

communications materials

ARTICLE

https://doi.org/10.1038/s43246-023-00410-2 OPEN

A multibody kinematic system approach for the design of shape-morphing mechanism-based metamaterials

Pier H. de Jong [1✉], A. L. Schwab[1], Mohammad J. Mirzaali [1✉] & Amir A. Zadpoor [1]

Shape-morphing structures have the ability to adapt to various target shapes, offering significant advantages for many applications. However, predicting their behavior presents challenges. Here, we present a method to assess the shape-matching behavior of shape-morphing structures using a multibody systems approach wherein the structure is represented by a collection of nodes and their associated constraints. This representation preserves the kinematic properties of the original structure while allowing for a rigorous treatment of the shape-morphing behavior of the underlying metamaterial. We assessed the utility of the proposed method by applying it to a wide range of 2D/3D sample shape-morphing structures. A modular system of joints and links was also 3D printed for the experimental realization of the systems under study. Both our simulations and the experiments confirmed the ability of the presented technique to capture the true shape-morphing behavior of complex shape-morphing metamaterials.

[1] Department of Biomechanical Engineering, Faculty of Mechanical, Maritime, and Materials Engineering, Delft University of Technology (TU Delft), Mekelweg 2, 2628 CD Delft, The Netherlands. ✉email: P.H.deJong@tudelft.nl; M.J.Mirzaali@tudelft.nl

Shape transformation or shape-morphing is a ubiquitous phenomenon in nature. Organic materials, such as clay, exhibit shape-morphing. Living organisms manifest such behaviors too. Examples are plants, such as codariocalyx motorius (or telegraph plants), venus flytraps, pine cones, or animals, such as octopuses with their tentacles or tree frogs and their toe pads[1–7]. Many biological materials can deform their bodies substantially without losing their integrity in a response to external stimuli, such as temperature, humidity, and predation. Shape-morphing then serves as a means to facilitate other biological processes. The microstructures of such biological materials are responsible for their (dynamic) shape-morphing behavior.

Shape-morphing has numerous applications in (high added value) industries[7]. These include architecture[8,9], furniture[10], automotive (interior[11], exterior[12]), soft robotics[13], and biomedical engineering. In those fields, we often tweak structures on the microscale to make them morph their shape in such a way that they can resemble the contour of another object. This type of shape transformation is useful when an object needs to maximize its contact area with another object (Fig. 1a). Changing the shape of grippers and fixtures to comply with the shape of the objects they grab onto or propel over helps in distributing the contact forces in the most favorable manner. To design shape-morphing objects that deliver the most favorable shape transformation properties, designers often resort to architected materials that are otherwise referred to as metamaterials[14].

Metamaterials allow us to design shape-morphing objects that incorporate other desired properties as well. Materials like clay are almost perfect in matching shapes, but are also continua. A more porous metamaterial could have the shape-morphing properties of clay but be lighter or offer other advantages afforded by its cavities (e.g., bony ingrowth in the case of orthopedic implants). Furthermore, an architected metamaterial makes it possible to realize effective (mechanical) properties that the base material used to create the metamaterial lacks. Shape-morphing metamaterials can, for example, fold (origami/kirigami)[15], bend[14,16], or deform through kinematic joints[17]. Here, we investigate the versatility of the shape-morphing behavior of such kinematic structures.

Kinematic structures can be created from highly stiff materials but still exhibit shape transformations[17,18]. One could, for example, connect (relatively) rigid parts through kinematic or compliant joints that are made from a base material with high stiffness. The complete structure then possesses the overall ability to easily adapt its shape. We see many manifestations of physical kinematic structures[17,18]. A successful design of a metamaterial with a "universal shape-morphing" behavior relies on the rational geometrical design of its connecting elements (i.e., links) and joints.

In this paper, we introduce a methodology to predict the shape-morphing behavior of architected kinematic structures. Through several examples, we illustrate the connection between this representation and physical phenomena. These predictions are essential because they enable an analysis of the envelope of possible shape transformations for any given design. Such an envelope of possible shapes can then be assessed in its own right.

Mobility describes the possible motions that an object can undergo. This number of motions is captured by the degrees of freedom (DoF) of the object. A single rigid body has six DoF in 3D: rotations around three axes and translations along three axes. A deforming body has more DoF: as many as there are isolated possibilities to deform. Solidly deforming objects have an infinite number of DoF and can, therefore, transform theoretically into infinitely many shapes. This is illustrated in Fig. 1a, b. Such structures are generally studied by finite element modeling (FEM)[19–22]. Kinematic structures, illustrated in Fig. 1c–e, have a limited number of DoF. The current designs and mathematical representations of shape-morphing structures often have limited mobility and can transform, or be deployed, from one starting shape into one final shape, as the final shape is programmed into the design of the mechanism[15,23–29]. The more DoF a structure has, the more shapes it can match. For a structure with limited mobility, it might be possible to predict the shapes it can attain. However, even with a limited number of DoF, a structure could match a vast number of different shapes. Simulations are needed to determine whether and how well a structure can deform into different shapes. To perform these simulations, we turn to the theory of rigid multibody systems.

Rigid multibody systems describe the motions of structures consisting of rigid bodies and (kinematic) joints. Since we are modeling kinematic structures, we need to make sure their integrity is not violated. In fields that deal with shape-morphing

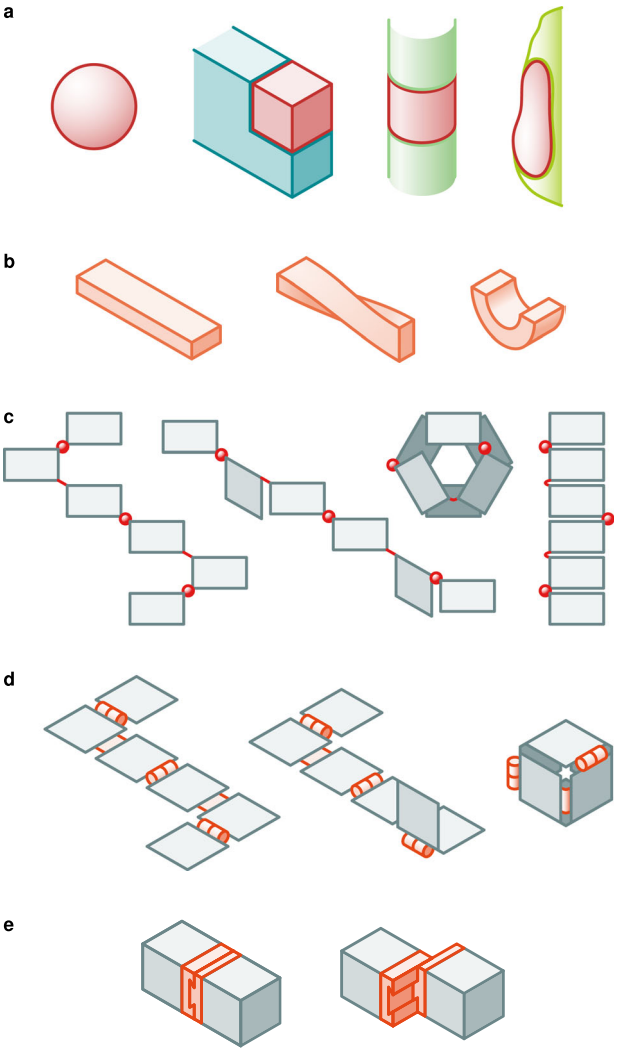

Fig. 1 An illustration of the ability of different structures to deform. a A solid deforming structure with an infinite number of DoF. A single structure can deform to take the shape of different substrates. **b** A solid deforming structure with an infinite number of DoF, which more easily deforms along specific directions. **c** A multibody structure with both kinematic and compliant spherical joints, providing it with many transformation DoF. **d** A multibody structure with both kinematic and compliant hinges, affording it by a few transformation DoF. **e** A multibody structure with prismatic joints, leaving one transformation DoF. In the multibody examples, the revolute hinges are represented by "cans"[42].

(*e.g.* (meshing) in computer graphics/vision[30–32]), shapes are often described using points and vertices. Combining this approach with multibody principles assures that such a mesh can also describe the motions of a physical structure. This would guarantee that the integrity of the structure is preserved and that the relations between the different sections of the structure are maintained during the whole process of shape transformation. This idea of using points motivates the use of a discrete multibody approach.

A discrete multibody approach defines the entire kinematic structure by looking at specific points of interest. This is a systematic and scalable approach that we adopt here because we are primarily interested in the kinematics and not so much in the kinetics of such architected materials. A morphing shape is said to resemble another shape when they share enough contact points. To match a discrete structure to a shape, one must move selected points within the structure toward their target locations. This discretization of solid bodies to points is already used in multibody dynamics[33–37]. Here, however, the approach is specifically tailored to study shape-morphing with as few nodes as possible. Such an approach also makes sure that kinematic structures can be modeled in a systematic way and that the obtained simulations are free from singularities. With this design representation, for any given target shape, we can determine how well a structure design is able to approach this shape. This could provide means to find combinations of design parameters that result in optimal designs. We assess the utility of the developed method by performing both simulations and experiments. The experiments are performed using an additively manufactured (AM or 3D printed) modular system that enables us to connect links and joints in arbitrarily complex ways, thereby creating many possible designs of kinematic structures.

Results

The simulation results corresponding to case studies show that the proposed design representation in the current study for modeling the shape-morphing behavior of kinematic structures works well in terms of finding the correct matching shape. The simulation and experimental results were generated by considering different sample structures that were specifically selected to showcase the different types of constraints and their associated shape-morphing behaviors. The kinematic structures used for the assessment of the morphing behaviors of the sample cases were created by defining their initial node positions and the constraints limiting the relative motions of the nodes according to the generally developed principles (see Section “Structure representation” in the Methods). Subsequently, a generally developed morphing algorithm (see Section “Morphing simulation” in the Methods) was applied to transform the shape of the mathematical structures into a desired one. The here presented morphing simulations and the experimental comparison with a physical representation follow study-specific methods (see Section “Case studies” in the Methods).

An overview of some sample structures and target shapes is presented in Fig. 2. Here, a 3D deforming “pentapod” is composed in such a way that it only has one morphing DoF (Fig. 2a). There is a rationally designed coupling between the nodes along different axes that makes this possible. Although the space in which the movements take place is 3D, we can apply hinges in such a way that only 2D in-plane morphing of structures is possible (Fig. 2b). This structure has multiple DoF because of the network of many hinges. A fully 3D defined structure with spherical joints has many DoF and can transform its shape into irregular 3D shapes (Fig. 2c).

In the specific examples considered here, not all nodes were moved toward the target surface. We selected the peripheral nodes of the structure as the “leading nodes” that moved toward the target shape. The inner nodes were initially allowed to stay close to their starting positions. The internal nodes followed the leading nodes only when they had to provide extra movements so that the leading nodes could approach their target positions.

The simulations confirmed the capability of the structures to transform into the specific target shapes. The “leading nodes” at the edges move toward the target shape. The nodes located at the center of the structures remained mostly in their original positions, if they did not have to accommodate the movement of the edge nodes. The residual error of the “pentapod” in (Fig. 2a) was relatively large as compared to the other examples. That is due to the fact that its target shape is irregular and the structure has effectively only one transforming DoF. Moreover, the pentapod showed “expansion” with increasing shape factor while the shape factor of both other structures reduced. These results can be used to improve the designs of these structures in terms of shape-morphing behavior and reduce the residual error.

A comparison between the simulated shape-morphing and the experimentally obtained shapes shows that they are in agreement with each other. The 2D structure could deform into a 1D circular shape (Fig. 3a), a 2D cylindrical surface (Fig. 3b), and a 3D ellipsoidal enclosure (Fig. 3c). The simulations predicted this, and although the physical dimensions and possible imperfections limited the range of motion of the physical structure, it could approximate the shape factor of the simulations.

Discussion

The multibody kinematic approach presented here provides the required steps for an initial configuration to morph into a target shape. This was initially demonstrated for different structures in a first set of simulations (Fig. 2). To illustrate the working principles of the approach further and demonstrate the physical realization and compare it with our simulation results, we analyzed the capabilities of the presented approach in predicting the shape-morphing steps required for several arbitrary shapes.

A second set of experiments showed how one single structure can morph into multiple shapes by simply defining different target shapes. We simulated the behavior of a 2D structure that morphs into various shapes in 1D, 2D, and 3D (Fig. 3). The simple structure consisted of two triangular bodies connected through spherical joints by a link. The same structure was morphed into three different target shapes, including a circular surface that made the structure deform in one plane along a line, a curved surface that made the structure morph into an out-of-plane shape, and an ellipsoidal enclosure that required the structure to deform into a 3D shape. The different target shapes of the substrates were purposely chosen to give the structure compelling end shapes. Situations occurred where the combination of structure and target shape was too symmetric, leading to bifurcations. Multiple routes to the target shape were equally ideal which can lead to longer calculation times and undesired structure configurations. To circumvent this, symmetry was removed by translating or rotating the target shape slightly with respect to the morphing structure in order to break the alignment of the symmetry axes of shape and structure.

In our physical representations, we followed the exact same steps obtained from our simulations and found that the resulting shapes matched the target shapes. We need to emphasize here that the 3D printed structures had length ratios that were identical to the simulated ones. However, these physical experiments also made it clear that the intermediate steps resulting from the simulations are primarily of theoretical value. The different steps

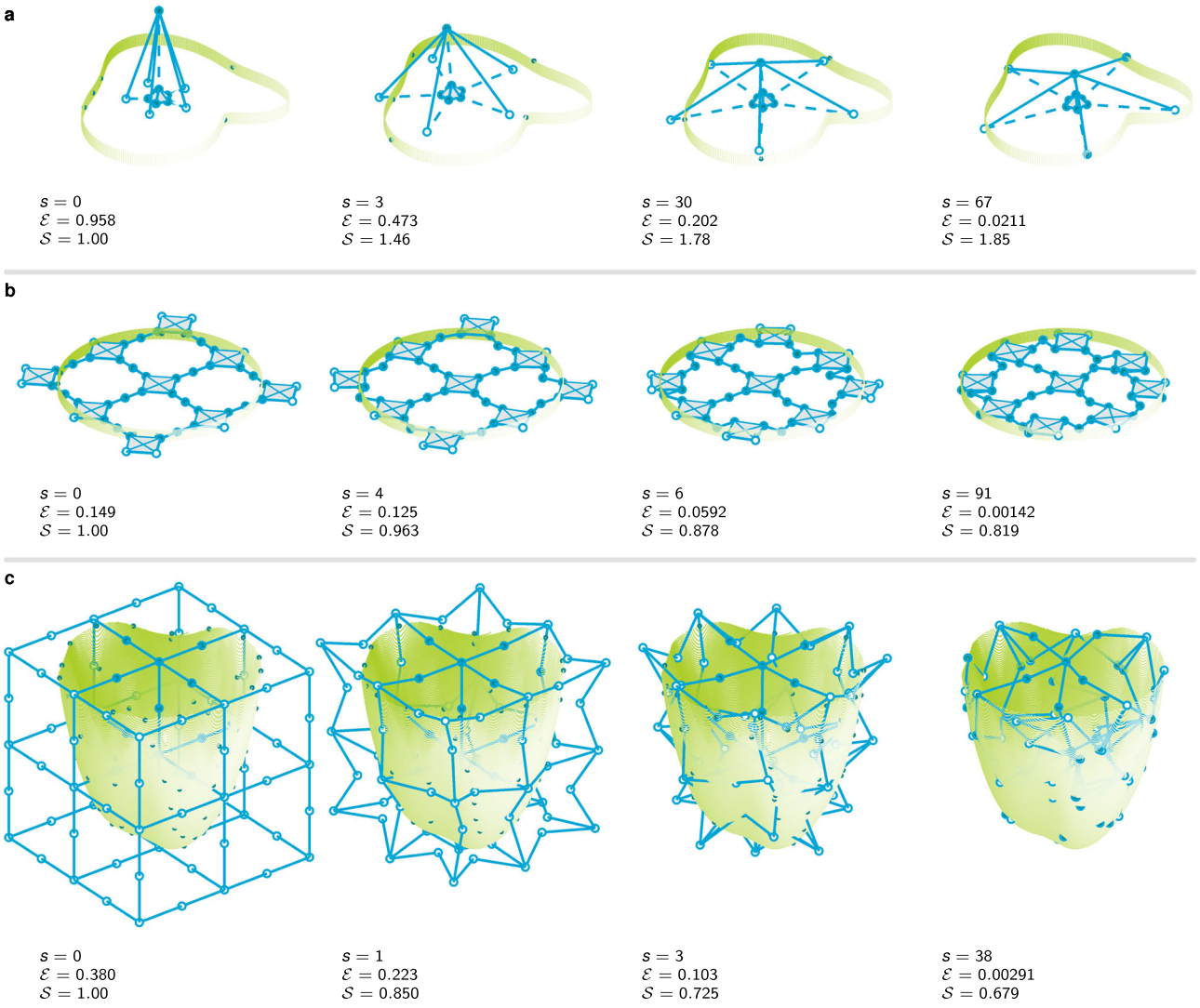

Fig. 2 Three sample applications of our shape-morphing simulations. Nodes are depicted by blue circles and links are represented by blue solid lines. Line-point joints are depicted by dashed lines. For a selection of steps s, the configurations with shape factor $\mathcal{S}$ is shown. The targets for the upcoming step are shown with dots. The distance error $\mathcal{E}$ indicates how far the current configuration is from the targets. **a** A "pentapod" matching its shape to a cylindrical surface with a randomly varying radius. Only the five outer nodes were moved toward the shape. Line-point constraints were used to make the outer nodes move in one plane (simultaneously). Next to the six DoF of the overall motion, this structure has only one shape-transforming DoF. **b** A structure with square bodies connected by hinging links[18] was morphed into a circular shape. Only the nodes on the edges were given target locations. Plane-point constraints were used to restrain all the nodes in one plane. **c** A 3D structure with spherical joints was morphed into an organically created 3D shape. Only the nodes on the bottom and side faces of the structure were given target locations.

obtained for the shape-morphing process represent the shortest trajectory from the initial shape to the target shape. This means that our simulations do not take into account all the physical properties of the joints. Some of the physical properties of joints and links, such as their thicknesses, can limit their actual range of motion. One way to apply such limits in the range of motion of a node without changing the current way of defining constraints is to add an additional node (Supplementary Note 3). The number and location of nodes that represent a body are chosen carefully in the experiments to represent a physical system while using as few nodes as possible. Adding nodes carelessly can make the calculations longer as well as giving undesired results (Supplementary Note 4).

We used a two-step Gauss-Newton iterative procedure to make sure the shape transformation trajectory was as close as possible to the actual physical situation. In this procedure, the nodes were moved toward their target first, followed by corrections that ensured the constraints were satisfied to the desired level of accuracy. The integrity of the system was, therefore, maintained during the shape transformation process. Had we solved the model simultaneously for both target-approaching trajectories and constraint satisfaction, different final configurations would have appeared that would have significantly deviated from what is physically possible. The physical "insertability" of such shapes would have, therefore, been less predictable. Doing the constraint satisfaction in a separate step of the iterative process is a more effective approach for maintaining the integrity of the kinematic structure as the shape transformation takes place. The final shape of the structure will then preserve its original topology.

Given that the primary purpose of the current paper is to propose a straightforward model for the study of the shape-morphing behavior of kinematic structures, we did not consider some more advanced aspects of kinematic structures, such as shape transformation in the presence of additional constraints

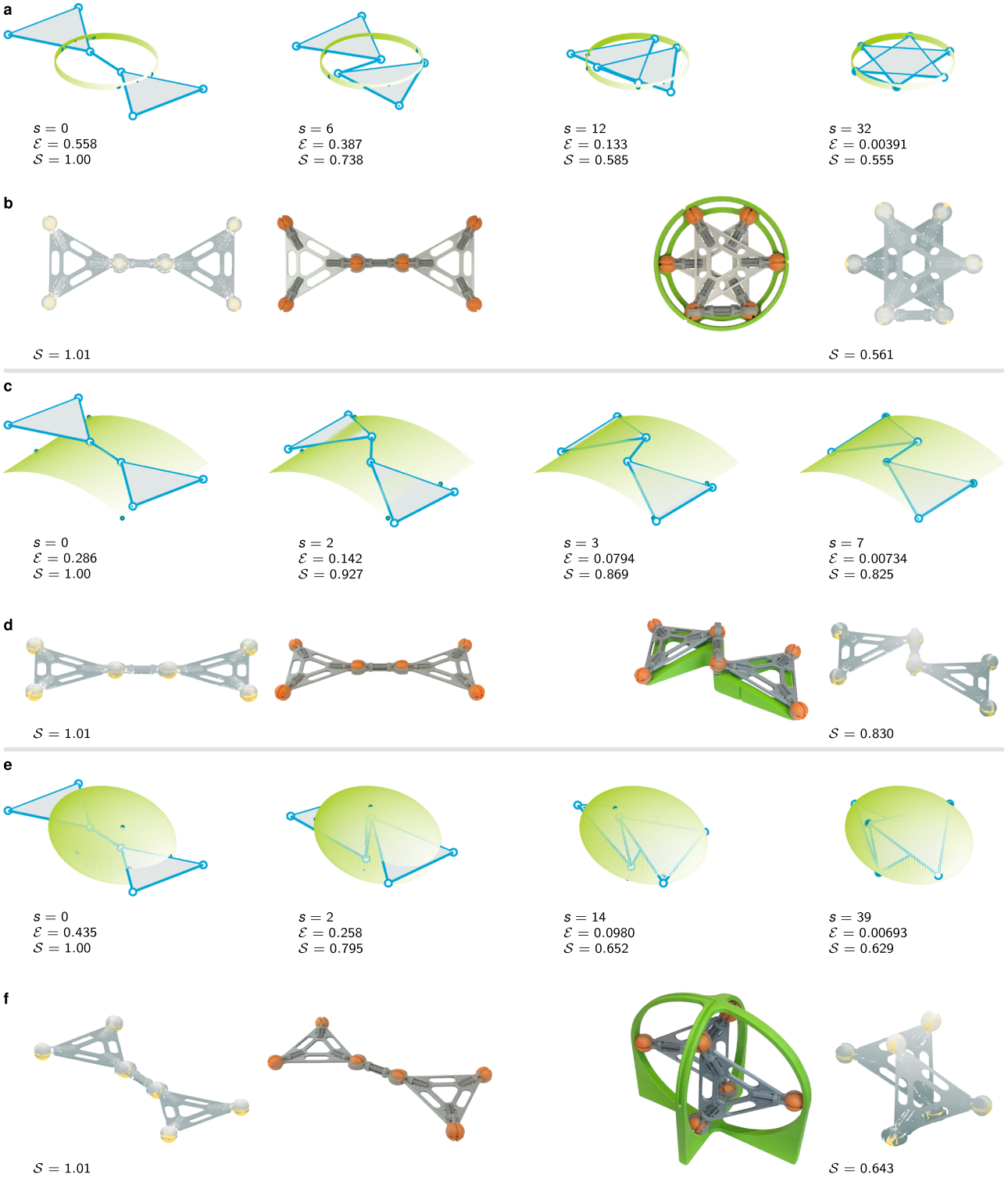

Fig. 3 Simulation of the transformation of the shape of a structure with triangular bodies into three different shapes. The target shapes are **a**, **b** a circle, **c**, **d** a cylindrical surface and **e**, **f** an ellipsoidal enclosure. In each case, the simulated behavior is shown for selected steps s along with the physical representation of the modular system corresponding to the initial and final configurations. The blue circular nodes are physically represented by orange spheres. The 3D printed structure's shape was captured using a 3D optical scanner. From the point cloud the yellow spheres were selected manually. Both the normalized error $\mathcal{E}$ between the structure and the substrate and the normalized shape $\mathcal{S}$ are presented. The simulations stopped once the absolute error difference $\bar{\mathcal{E}}$ was below $1 \cdot 10^{-6}$. All the values were normalized with respect to a characteristic length which was chosen to be a representative value of the initial shape at $s = 0$.

that limit the range of motion of individual joints. Every joint could, therefore, move freely along its DoF. In reality, however, the physical nature of a structure limits the range of motion of different joints in a joint- and location-specific manner.

The primary limitation of the proposed method lies in the simplifications that make it somewhat deviate from the actual physical situation. In particular, rigid bodies were simply defined as a collection of theoretical nodes without volume. In the real world, physical bodies occupy volume and cannot penetrate into each other[38,39]. These aspects have not yet been included in the presented modeling approach. The finite dimensions of the physical structures and the limited range of motions of joints are the other aspects missing from our approach. These omissions mean that one needs to be careful about the selection of the nodes that lie on the surface and the ones that do not. For a qualitative assessment of the shape-morphing behavior, this does not pose a problem but any quantitative results may be less accurate than those of more complex models.

The current version of the proposed method is also purely kinematic, meaning that stiffness is excluded from the equations. The elements of the model are, thus, either fully rigid –and thus non-deformable– or fully free to move along their DoF. Rigid bodies are, therefore, assumed to possess infinite stiffness while joints are inferred to have zero stiffness. To study how compliant bodies and joints contribute to the shape-morphing behavior of physical structures, we need to introduce forces. A theoretical spring with a finite stiffness does not limit the motion of a point in a multibody model. In reality, however, it limits the deformation that is possible without material failure. Moreover, it can also contribute to mobility through the deformation of parts that are considered rigid in this multibody approach. By introducing masses and/or stiffness values[40] into the system, it would be possible to investigate the reaction forces at different joints. Static forces in the system can then be calculated by evaluating the local stiffness in-between the nodes. This would be somewhat similar to FE modeling. It is important to emphasize that while multi-step simulations make it look like the kinematic structures move toward their targets, this should not be misinterpreted as a dynamic analysis. This movement purely represents the kinematically optimal path (i.e., the path with the shortest least-square distance) that satisfies the imposed constraints. It is possible to extend the presented node-and-constraint model to include kinetics. The bodies would then need to have at least four nodes with assigned masses to be able to manifest the full kinetic effects of their mass and moments of inertia. Implementing non-rigid bodies is possible within the current modeling framework by simply assigning stiffness values to the links.

To modify the model, one can change the way through which we find the final position of nodes. In the presented method, the nearest point on a surface was used, but this can be changed to other norms, such as the 1-norm, a projection along an axis, or the Hausdorff distance[41]. These methods have been used in computer graphics algorithms[31] that have many similarities to the algorithm presented here. Another note regarding the search for the target coordinates is that representing the target shape as a point cloud makes the search computationally much more expensive than if the target shape was represented by a function. It is, therefore, advised to use a functional representation of the target shape, as this would allow for more computationally efficient handling of the function minima.

Conclusions

We proposed a simple method for the study of the shape-morphing behavior of kinematic structures. We then applied this design representation to a number of cases to demonstrate its utility in predicting the shape-morphing behavior of a large class of architected materials consisting of links, bodies, and joints with various DoF. The simulation and experimental results obtained for the case studies confirmed the ability of the proposed technique to match kinematic structures to arbitrary shapes through a variety of mechanisms. The presented approach, therefore, provides us with a way of determining a structure's ability to transform into arbitrary shapes particularly when the target shape is complex and does not lend itself to other more rudimentary techniques of shape analysis. The methodological advances made through the proposed technique pave the way for more systematic investigations of shape-morphing phenomena, including the determination of the envelope of the shape-morphing behaviors that can be exhibited by any given kinematic structure. Such information would be also essential for the algorithmic optimization of kinematic structures with the aim of making them morph into any specific classes of shapes or for enlarging the envelope of possible achievable shapes as much as possible.

Methods

Structure representation. The shape-morphing model proposed here consists of two main components, namely nodes and constraints, with which the mobility of structures can be fully described. Using this discrete approach, the overall configuration of the structure is simply defined by evaluating the local displacements of individual nodes in the 3D space. The analysis starts by expressing the system in terms of nodes and constraints. Subsequently, we find the possible motions of individual nodes and transform the complete system into a target shape that is defined as the superposition of the local motions of individual nodes. Further information on the kinetics of the system (i.e., force and moments at individual nodes and links) can be also inferred from this approach but is outside the scope of the present study.

The mathematical description of a system with such few types of elements is relatively straightforward and systematic, and relies on positional descriptions provided by vectors and the applicable vector algebra. Figure 4 illustrates the usage of vectors for such mathematical descriptions. For each obstructed DoF, we define a constraint c that vanishes at all times (i.e., $c = 0$). In what follows, we describe the theoretical model by going from a single node towards a full multibody system with different joints and a large number of DoF.

Nodes, links and bodies. Nodes are the basic elements in the description of our multibody systems and define the primary points of interest. Moreover, constraints are written in terms of the relative motions of nodes. The relative fixation and motion of nodes can all be described in terms of vectors. A single node has no dimensions. It, therefore, has only three DoF, including translations along the x-, y-, and z-axis. The coordinate of a node "1" is then defined as (Fig. 4a)

$$\mathbf{r}_1 = \begin{pmatrix} x_1 & y_1 & z_1 \end{pmatrix}^{\mathrm{T}}. \tag{1}$$

Each system can be modeled using n nodes whose relationships with each other are described by m constraints. The overall number of DoF of the system f can then be approximated as: $f = 3n - m$. Multiple constraints may remove the same DoF. This approximation may, therefore, not hold exactly. To describe the relative motion between different (subsets of) nodes, we use the node locations and relate them to each other.

Links are defined as a constant distance between two nodes (Fig. 4b). Such a constraint removes one DoF from the set of nodes. Therefore, a link has five DoF and can be considered as a simplified body where the rotation is undefined along the link

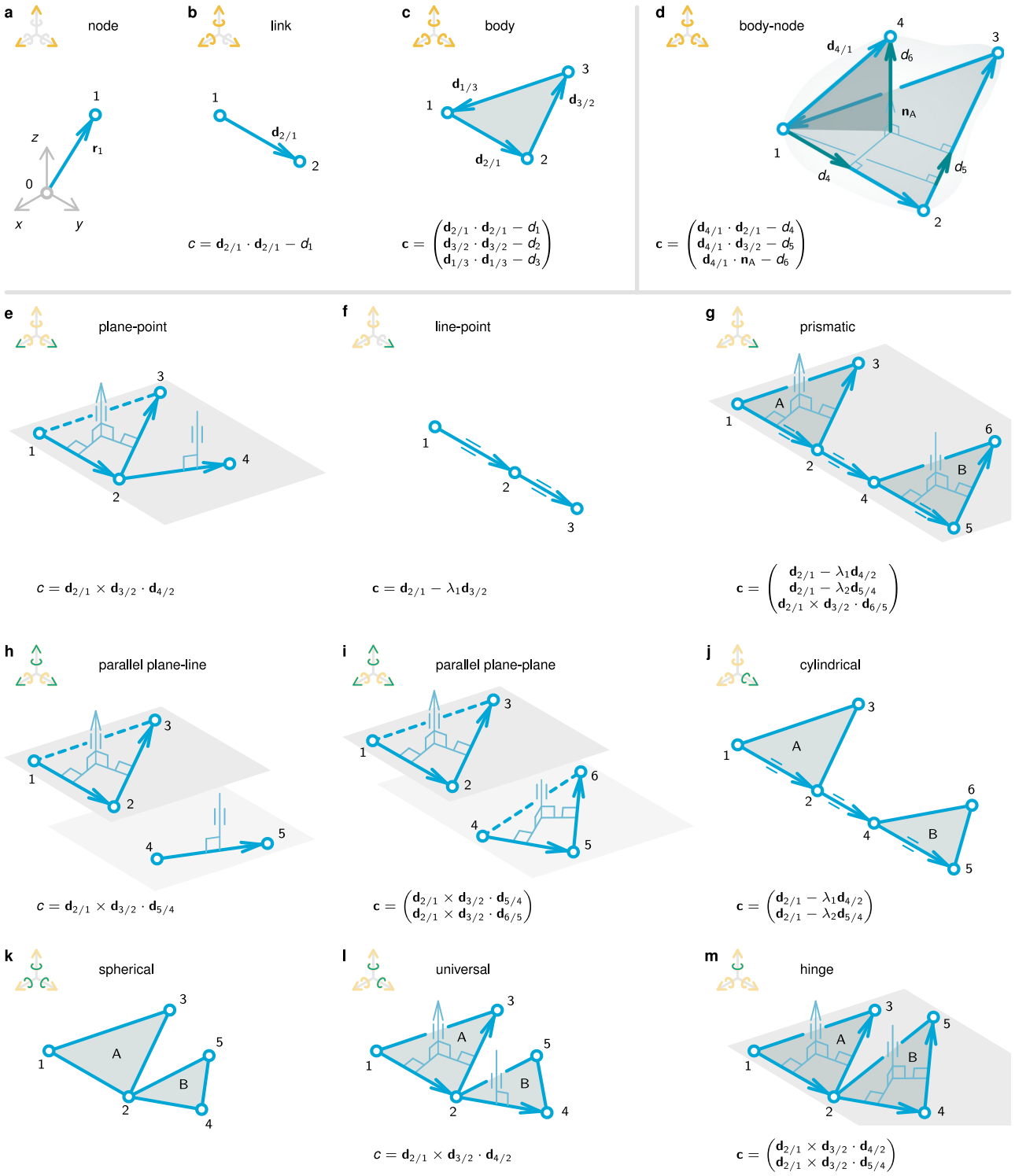

Fig. 4 Description of the nodes and constraints as the building blocks of our modeling approach. Based on a multibody analysis of kinematic systems, three rigid elements are considered: **a** A single node has three DoF, **b** A link is created by constraining the distance between two nodes, leaving five DoF, **c** Linking three nodes creates a body with six DoF. **d** Nodes are rigidly added to a body through projections on a normal vector and the sides of the base plane. **e**–**m** Different kinds of constraints and joints can be applied in-between bodies by using orthogonal and parallel vectors. The presented list of nine examples is non-exclusive and non-exhaustive. Depending on the situation at hand, the same relative motions can be defined in different ways and more constraints can be defined in terms of the relative motions of the system components. The triads depict the possible motions, either absolute (yellow) or relative to another body (green).

axis. To mathematically describe a link, the length of the vector from one node to the other needs to be set equal to a constant. As is shown in Fig. 4b, this is done through the constraint c. With the relative vector between both nodes defined as $\mathbf{d}$, the rigid link can be formulated as $\mathbf{d} \cdot \mathbf{d} = d$, where d is a prescribed constant of the link. The constant value of d is, thus, calculated in the original undeformed state. Since constraints need to always vanish, they are written as $c = \mathbf{d} \cdot \mathbf{d} - d = 0$.

Bodies are composed of three out-of-line nodes whose relative positions are rigidly constrained (Fig. 4c). This is the simplest form of a rigid body, since it requires the minimum number of nodes for a fully defined set of six DoF. The (sub)system of nodes creating a rigid body has a position as well as orientations along and about all three axes. In order to not prioritize any node over another, the vectors are simply drawn in a head-tail fashion. Any other choice in which all nodes are related to each other would be acceptable too.

The three components defined above (i.e., nodes, links, and bodies) are needed to define any other relationships between the nodes. From here on, we describe two mutually compatible ways separately. First, the body is extended with more nodes than the base three. Secondly, we combine nodes with links and/or bodies in order to generate large shape-morphing structures. In a structure, we can encounter both simultaneously. Structures could have bodies with more than three nodes and many different joints between their elements.

Body-node. The number of nodes of a body can be extended beyond three (Fig. 4d). However, singularity issues may arise when distance constraints are used for the extra nodes positioned within the plane formed by the three base nodes. We, therefore, had to find a way to attach the extra nodes while avoiding such singularities. Fortunately, the base body can be used to define the normal vectors in such a way that singularity is avoided.

We propose to extend a body's nodes beyond three by projecting the relative distance vector of the extra nodes onto the vectors related to the base plane. We start by separately projecting the relative distance vector on either two of the three base plane vectors. This provides us with two constraints. The remaining constraint is then obtained by setting the normal distance to the plane using the base plane's normal vector. To construct the normal vector, two separate vectors of the base are used (e.g., $\mathbf{n} = \mathbf{d}_{2/1} \times \mathbf{d}_{3/2}$).

Kinematic joints. Kinematic joints, or kinematic pairs, were introduced between nodes, links, and bodies to create transformation mechanisms. Every joint within a kinematic structure allows for a certain type of motion between the nodes of the system. There are many possible joint types of which nine examples are presented in Fig. 4e–m. This list of examples is non-exhaustive and serves solely to illustrate the principles. The relative nodal behavior of such joints can often be expressed through different definitions of constraints depending on what is most convenient in any specific case. The general idea, however, remains the same in all cases: the joints are mathematically described by constraining the movement of vectors with respect to each other.

One of the basic examples of joints that only confines translation is the plane-point joint (Fig. 4e). This joint blocks the relative translation of any arbitrary node (e.g., 4 in this particular example) with respect to a node of the plane of a rigid body. We, therefore, need a single constraint to describe this joint type. This constraint includes the normal vector of the plane that is found by taking the cross-product of two vectors of the plane. Subsequently, a third vector from a plane point towards the to-be-constrained point is projected on the normal vector. Since this projection is set equal to zero, the vector is orthogonal.

The next example of a basic joint is the line-point joint. This joint does not involve orthogonal vectors but is, instead, based on parallel vectors. The idea behind this choice is that a minimum number of nodes would be required as compared to the case where orthogonal vectors are used. These orthogonal vectors would need to be normal to the line and need an extra node to be robustly defined[34]. This is a result of the hairy-ball theorem and stems from the fact that a line has an infinite number of orthogonal vectors (Supplementary Note 1). We circumvent this issue by making the vectors parallel but not necessarily equal in length. For the line-point joint, one of the vectors defines the line while the other defines the position of the third node with respect to one of the other nodes (Fig. 4f). Both vectors are subtracted from each other to make them parallel and an extra DoF is added in the form of a multiplier λ. Eventually, this joint has three constraints but also introduces an extra DoF. The net effect of the joint, therefore, is to remove two DoF from the system.

A prismatic joint allows for relative translation between bodies (Fig. 4g). It uses two line-point constraints and a parallel plane-line constraint. This last constraint is very similar to the plane-point joint with the difference that the vector does not originate from the body. This allows for translations as well as rotations. Other joints that allow for both rotations and translations are the parallel plane and cylindrical joints. Joints that only allow for rotation are the spherical, universal, and hinge joints. The basic elements of orthogonal and parallel vectors provide the means to define the most common types of engineering joints.

System description. Kinematic structure are fully described through their instantaneous configuration and the constrained motions between their nodes. The overall configuration of the system can be described using two main sets containing n nodal coordinates and k multipliers:

$$\mathbf{x} = \begin{pmatrix} \mathbf{r}_1^{\mathrm{T}} & \mathbf{r}_2^{\mathrm{T}} & \dots & \mathbf{r}_n^{\mathrm{T}} \end{pmatrix}^{\mathrm{T}}, \tag{2}$$

$$\boldsymbol{\lambda} = \begin{pmatrix} \lambda_1 & \lambda_2 & \dots & \lambda_k \end{pmatrix}^{\mathrm{T}}. \tag{3}$$

The mathematical relations between all these nodes are the constraints that are stored in an $m \times 1$ constraint set:

$$\mathbf{c} = \begin{pmatrix} c_1 & c_2 & \dots & c_m \end{pmatrix}^{\mathrm{T}} = \mathbf{0}. \tag{4}$$

These constraints, which are usually nonlinear in $\mathbf{x}$, make sure that the configuration of the system remains within the kinematic limitations of the structure, thereby safeguarding the overall integrity of the structure during motions.

Morphing simulation. Once all the nodes and constraints are defined, kinematic transformations can be analyzed. The simulation has to be performed in an iterative manner from a start configuration toward a target configuration. This iterative algorithm uses the coordinates of a target shape and minimizes the difference between the current configuration of the structure and the target one. This process continues as the structure goes through successive steps, s, that gradually bring it closer to the target shape. The simulation stops when the change in the configuration is negligible and the algorithm is said to have converged.

We require a measure to assess the difference between the current shape and the target one[31]. For that, we adopted the normalized distance error between the current configuration of all nodes, $\mathbf{r}_j$, and their target configuration, $\mathbf{g}_j$, which is defined as:

$$\mathcal{E} = \frac{1}{L}\sqrt{\frac{1}{n}\sum_{j=1}^{n}(\mathbf{r}_j - \mathbf{g}_j)\cdot(\mathbf{r}_j - \mathbf{g}_j)}, \tag{5}$$

where n is the total number of nodes and L is a characteristic length of the structure. This metric effectively measures the standard deviation of the distances between the locations of individual nodes and their target locations.

To assess the achieved shapes, we introduced a nondimensionalized shape factor, $\mathcal{S}$. The error defined in (5) measures how well a structure matches a target shape but does not tell us how

the different shapes of a structure compare to each other. We, therefore, defined the shape factor such that it measures the standard deviation of the node locations from the instantaneous centroid of the structure:

$$\mathcal{S} = \frac{1}{L}\sqrt{\frac{1}{n}\sum_{j=1}^{n}\left(\mathbf{r}_j - \frac{1}{n}\sum_{j=1}^{n}\mathbf{r}_j\right)\cdot\left(\mathbf{r}_j - \frac{1}{n}\sum_{j=1}^{n}\mathbf{r}_j\right)}, \tag{6}$$

where $\frac{1}{n}\sum_{j=1}^{n}\mathbf{r}_j$ is the instantaneous centroid of the structure while L is a characteristic length of the structure. While this number may be the same for highly different structures, it allows for a quick first comparison between different shapes.

The iterative process of morphing the structure continues until the configuration does not change anymore. We can choose to evaluate either $\mathcal{E}$ or $\mathcal{S}$ to decide whether the end configuration has been reached. Here, we measured the absolute difference in error with respect to a step, $\bar{\mathcal{E}} = |\mathrm{d}\mathcal{E}/\mathrm{d}s|$, and repeated the process until $\bar{\mathcal{E}}$ was within a specified tolerance. This process is illustrated in Fig. 5.

Goal coordinates. Every node, $\mathbf{r}_j$, needs to have a target location $\mathbf{g}_j$. We adopted a method where the target points are chosen based on the Euclidean distance (2-norm) between the node and a target shape. As seen in Fig. 5a, the structure starts off with an initial configuration $\mathbf{x}$ (no multiplier constraints). A to-be-morphed-to shape is defined by the target configuration $\mathbf{x}_g$. In most shape-morphing instances, the exact target location of each node is not known beforehand. The target configuration can be updated after each step based on the actual configuration of the structure. These instantaneous target locations are stored in a vector $\mathbf{x}_g$. Note that $\mathbf{x}_g$ always has a size of $3n \times 1$ but does not necessarily need the targets specified for each node. It is also possible to provide a certain set of new location targets for the "leading" nodes, while the target locations of the other nodes remain unchanged. The "leading" nodes will then move towards the new position while "pulling" the remaining nodes with them.

Mobility. A multibody system with f degrees of freedom has at least f independent ways to deform. To investigate mobility, all these possible motions will be evaluated both in isolation and in combination with each other. The independent modes of motion are the possible sets of variations in the node coordinates. For a structure undergoing a 2D motion, the modes are shown in Fig. 5b. Having defined the constraints in the form of equation (4), we can find all the small variations which satisfy the constraints using the first derivative of (4) as:

$$\mathbf{J}\begin{pmatrix}\mathbf{U}\\ \mathbf{\Psi}\end{pmatrix} = \mathbf{0}, \tag{7}$$

where $\mathbf{J}$ is the $m \times (3n + k)$ Jacobian of the constraints and $\mathbf{U}$ and $\mathbf{\Psi}$ are matrices with its null spaces. The Jacobian is calculated as

$$\mathbf{J} = \begin{pmatrix}\partial\mathbf{c}/\partial x_1 & \partial\mathbf{c}/\partial y_1 & \ldots & \partial\mathbf{c}/\partial z_n & \partial\mathbf{c}/\partial\lambda_1 & \ldots & \partial\mathbf{c}/\partial\lambda_k\end{pmatrix} \tag{8}$$

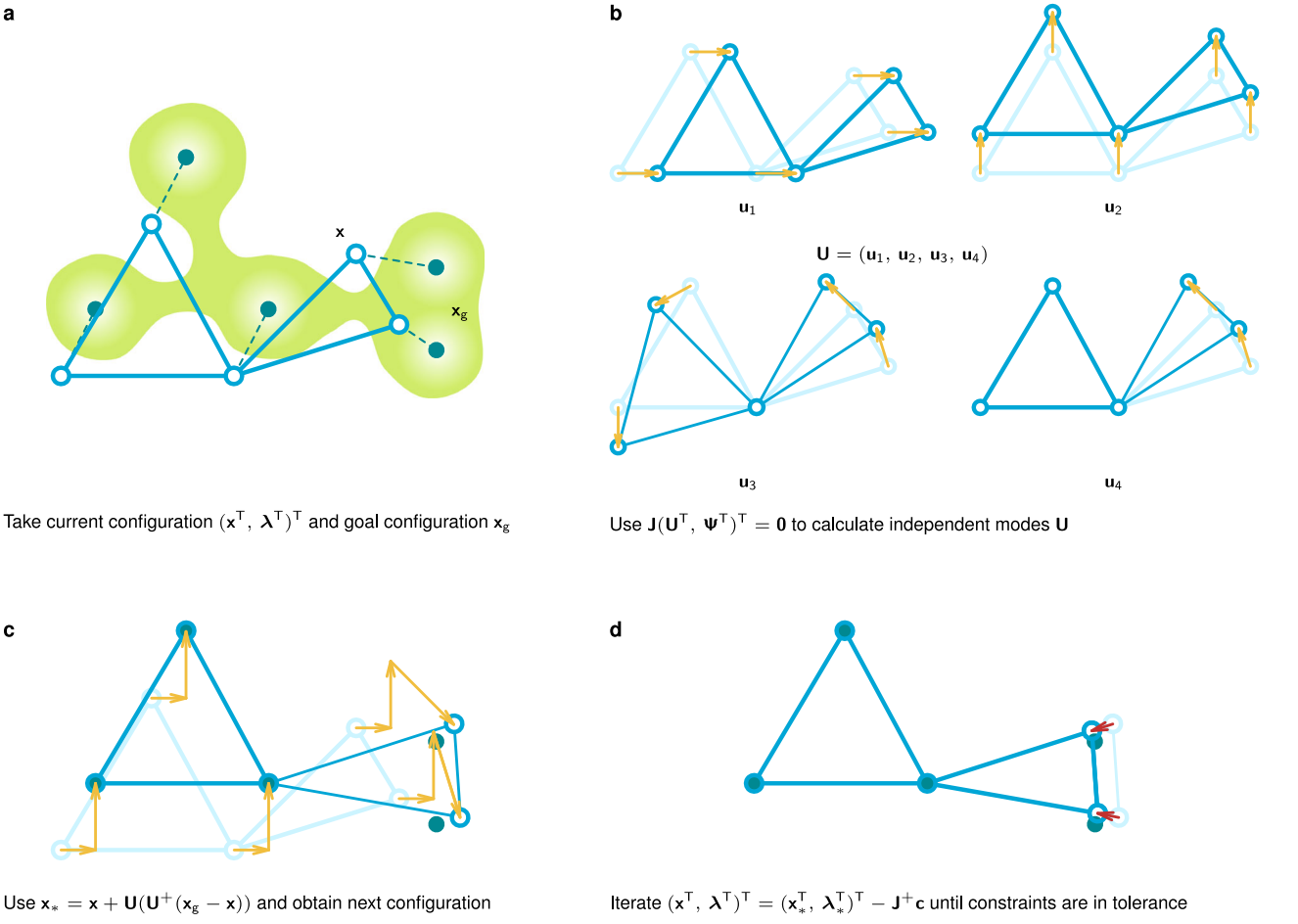

Fig. 5 An illustration of the steps involved in the shape-morphing algorithm that is applied to a structure moving in 2D. The target of each node is to reach the nearest bump on the surface as seen from the top view. The process iterates through steps **a**–**d** until the shape error derivative $\bar{\mathcal{E}}$ is below a predefined threshold.

while the null space can be subsequently determined using singular value decomposition (SVD). The columns of the Jacobian represent small deviations that are combinations of coordinate variations and can take place simultaneously. The separated modes containing the admissible variations of $\mathbf{x}$ and $\boldsymbol{\lambda}$ are then the null spaces:

$$\mathbf{U} = \begin{pmatrix} \mathbf{u}_1 & \mathbf{u}_2 & \cdots & \mathbf{u}_f \end{pmatrix}, \tag{9}$$

$$\boldsymbol{\Psi} = \begin{pmatrix} \boldsymbol{\psi}_1 & \boldsymbol{\psi}_2 & \cdots & \boldsymbol{\psi}_k \end{pmatrix}. \tag{10}$$

Modal superposition. Modal superposition is used to move and deform the structure to a desired configuration. In this way, the nodes move along linear paths that are admissible by the constraints up to the first order (Fig. 5c). We selected and combined the admissible motions stored in $\mathbf{U}$ by minimizing the distance that the nodes travel towards their target $\mathbf{x}_g$. Then, at each step of the motion, a change in the current configuration leads to the creation of a new configuration according to the following relationship (Supplementary Note 1):

$$\mathbf{x}_* = \mathbf{x} + \mathbf{U}(\mathbf{U}^+(\mathbf{x}_g - \mathbf{x})), \tag{11}$$

where $\mathbf{U}^+ = (\mathbf{U}^T\mathbf{U})^{-1}\mathbf{U}^T$ is the left pseudo-inverse of $\mathbf{U}$ and both $\mathbf{U}$ and $\mathbf{U}^+$ are evaluated in $\mathbf{x}$. Note that the variations in $\boldsymbol{\lambda}$ are not used in the modal superposition. Since the obtained information regarding the motions is a linear approximation, multiple steps are generally required to move to a new configuration while satisfying all the applicable constraints.

Constraint satisfaction. In each step, the nodes make a small linear movement with respect to their initial configuration that tends to slightly violate the constraints of the structure. As the number of steps increases, these initially negligible errors accumulate, requiring corrective measures. In fact, nodes that are part of bodies follow a curved path that cannot be described with a linear movement. Therefore, in each step, a constraint satisfaction step in the form of a Gauss-Newton algorithm is applied to the coordinates $(\mathbf{x}_*^T, \boldsymbol{\lambda}_*^T)^T$ to guarantee the constraints are satisfied up to a permissible residual (Fig. 5d). These corrections lead to new actual configurations after each step, which are given as (Supplementary Note 1):

$$\begin{pmatrix} \mathbf{x} \\ \boldsymbol{\lambda} \end{pmatrix} = \begin{pmatrix} \mathbf{x}_* \\ \boldsymbol{\lambda}_* \end{pmatrix} - \mathbf{J}^+\mathbf{c}, \tag{12}$$

where $\mathbf{J}^+ = \mathbf{J}^T(\mathbf{J}\mathbf{J}^T)^{-1}$ is the right pseudo-inverse of the constraint Jacobian $\mathbf{J}$ and $\mathbf{c}$ includes the constraint errors, both evaluated in the configuration $(\mathbf{x}_*^T, \boldsymbol{\lambda}_*^T)^T$. The constraints with $\boldsymbol{\lambda}$ are affected as well and need to be corrected too. These corrections are performed in an iterative manner (within the overall iterative process) to guarantee the satisfaction of the constraints up to a permissible residual.

Case studies. Experiments are conducted to illustrate and validate the usage of the approach. Simulations show how different structures can be implemented and transformed into different shapes. A reconstruction with a physical modular system shows how the simulations compare to the physical world.

Simulations. For the simulations, the target shapes are point clouds that are either created through the direct applications of mathematical expressions or by converting a CAD drawing. Shapes with constant (Gaussian) curvature are created with straightforward functions. To create more irregular surfaces, we used Fourier expansions. While the CAD drawing that is used here as one of the sample shapes is hand-drawn, any real-world physical objects could be handled similarly. The only additional step would be some type of 3D scanning.

Two parameters were defined to run the simulations. In all the simulations performed here, the characteristic length is given by:

$$L = \sqrt{\frac{1}{n}\sum_{j=1}^{n}\left(\mathbf{r}_{j0} - \frac{1}{n}\sum_{j=1}^{n}\mathbf{r}_{j0}\right)\cdot\left(\mathbf{r}_{j0} - \frac{1}{n}\sum_{j=1}^{n}\mathbf{r}_{j0}\right)}, \tag{13}$$

where we use the initial structure node configurations, $\mathbf{r}_{j0}$, such that $\mathcal{S} = 1$ at $s = 0$. Moreover, all the simulations stopped when $|\bar{\mathcal{E}}| < 1 \cdot 10^{-6}$.

Modular physical system. To illustrate and validate the capability of the presented modeling approach, we designed a modular system to recreate some of the various joint types discussed here as physical models and demonstrate their physical kinematic motions (Fig. 6a–e). In the created modular system, spheres represent nodes in kinematic systems. These spheres were connected to different parts to create rigid bodies that allowed for different types of motion variations. The rigid body shapes can be combined with different joint types to form shape-morphing structures (Fig. 6f). We used 3D printers to fabricate our physical models (Supplementary Note 2). Different pieces were combined to make different kinematic joints and structures with different shape-morphing behaviors. The spheres were printed using stereolithography (SLA) printers (Form 3, Formlabs, United States; color resin). The spheres were connected to each other to create links and bodies. Links were printed using SLA (Formlabs gray resin) while ridged shafts and bodies were printed using fused deposition modeling (FDM) (Ultimaker 2+, Ultimaker, The Netherlands; silver metallic filament). Different circular clamping pieces were made with SLA (Formlabs tough 1500 resin) which could be snapped around or into the ridges of the spheres. The shapes of these clamps determine whether or not they can rotate and with how many DoF. Different combinations of circular pieces create either a fixed, spherical, hinge, universal, or hinge connection around the sphere. The shafts are snapped into the other ends of the circular pieces. Furthermore, the shafts are snapped into tubes to create cylindrical or prismatic joints, where the prismatic joints make use of the ridges of the shafts to block any rotations.

The modular system was first evaluated for a specific structure whose morphing behavior is quite intuitive and was similarly captured by both simulations and experiments. This allowed for a comparison between the shape as predicted by the model and the physically realized shape. The model yielded the final positions of the nodes and the corresponding shape value. The physical representation of the system was put into different shapes and its node locations were recorded.

Target shapes. Target shapes were physically created for the validation experiments as well (Ultimaker 2+, Ultimaker, The Netherlands; green filament). They have an open structure that provides the opportunity to capture the structure once it is placed on or in the target shape. The three shapes are a circle, a cylindrical surface, and an ellipsoidal enclosure, which were sized to be compatible with the simulations (Supplementary Note 2).

Configuration capturing. As for capturing the positions of individual nodes, we used a 3D optical scanner (Scan-in-a-Box-FX, Open Technologies S.r.l., Italy) and extracted the coordinates of the nodes by manually selecting the spheres from the 3D scanned point clouds. Then, the shape factor was calculated and compared between our simulations and the physical model.

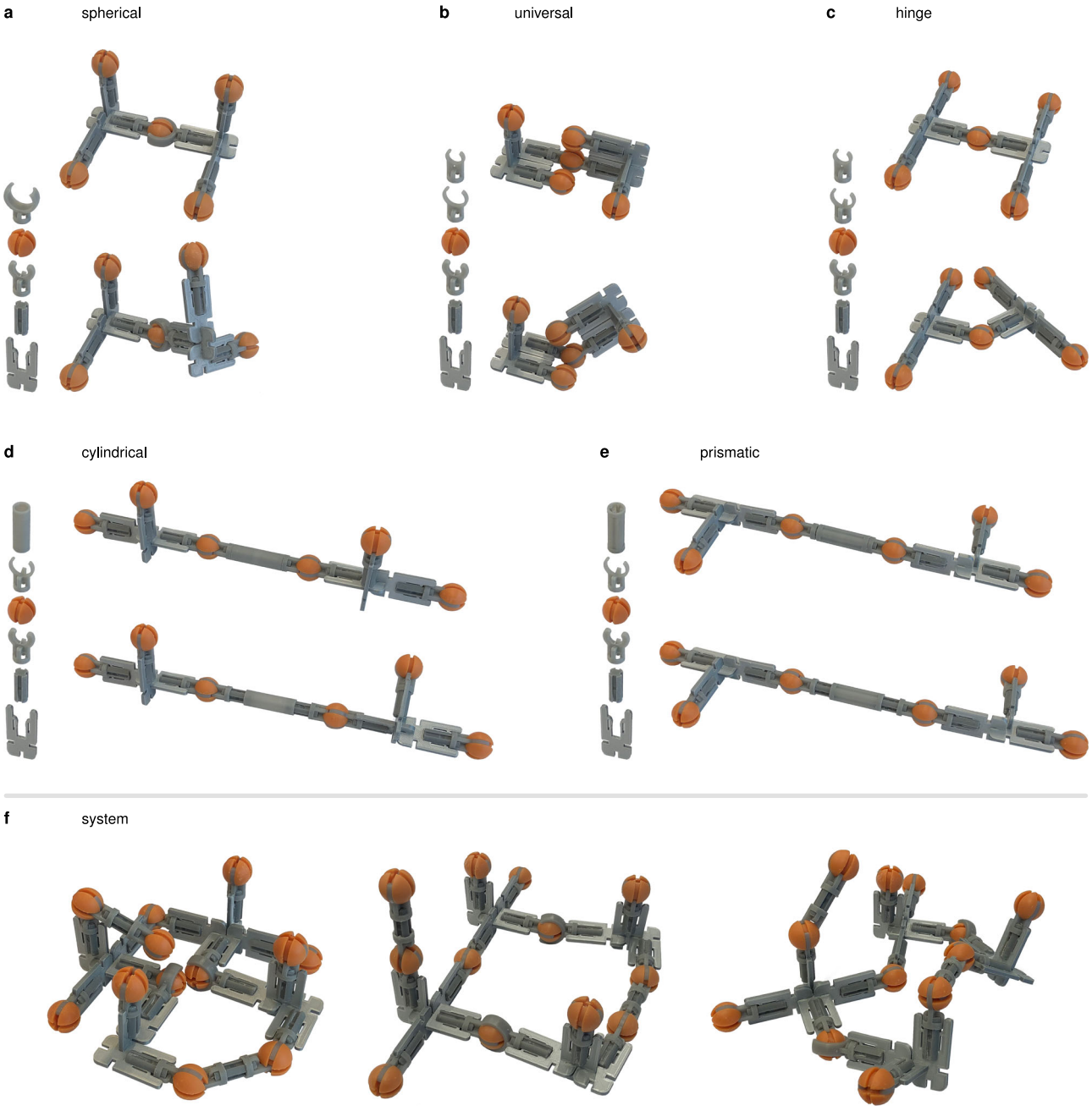

Fig. 6 A modular system illustrating the physical behavior of multibody systems. a–e Five common kinematic joints. The modular pieces were used in different combinations to create the different behaviors of the structures. The spheres were placed such that they can be easily used in mathematical definitions of the joints. **f** Different kinematic joints were combined to create versatile systems, including both closed-loop systems and systems with open ends.

The characteristic length for all cases (simulation and scanning) was that of the simulation's initial configuration as calculated with (13).

Received: 24 January 2023; Accepted: 22 September 2023;
Published online: 09 October 2023

Data availability

Data supporting the findings of this study are available from the corresponding author upon reasonable request.

Code availability

Code supporting the findings of this study are available from the corresponding author upon reasonable request.

References

1. Laschi, C. et al. Soft robot arm inspired by the octopus. *Adv. Robot.* **26**, 709–727 (2012).
2. Volkov, A. G. (ed.) *Plant Electrophysiology* (Springer, 2012).
3. Studart, A. R. & Erb, R. M. Bioinspired materials that self-shape through programmed microstructures. *Soft Matter* **10**, 1284–1294 (2014).
4. Oliver, K., Seddon, A. & Trask, R. S. Morphing in nature and beyond: a review of natural and synthetic shape-changing materials and mechanisms. *J. Mater. Sci.* **51**, 10663–10689 (2016).

5. Langowski, J. K. A., Dodou, D., Kamperman, M. & van Leeuwen, J. L. Tree frog attachment: mechanisms, challenges, and perspectives. *Front. Zool.* **15**, 32 (2018).
6. Poppinga, S., Correa, D., Bruchmann, B., Menges, A. & Speck, T. Plant movements as concept generators for the development of biomimetic compliant mechanisms. *Integr. Comp. Biol.* **60**, 886–895 (2020).
7. Ren, L. et al. Plant-morphing strategies and plant-inspired soft actuators fabricated by biomimetic four-dimensional printing: a review. *Front. Mater.* **8**, 651521 (2021).
8. Fiorito, F. et al. Shape morphing solar shadings: a review. *Renew. Sustain. Energy Rev.* **55**, 863–884 (2016).
9. Li, Y., Zhao, Y., Chi, Y., Hong, Y. & Yin, J. Shape-morphing materials and structures for energy-efficient building envelopes. *Mater. Today Energy* **22**, 100874 (2021).
10. Grønbæk, J. E., Korsgaard, H., Petersen, M. G., Birk, M. H. & Krogh, P. G. Proxemic transitions: designing shape-changing furniture for informal meetings. In *Proce. 2017 CHI Conference on Human Factors in Computing Systems* 7029–7041 (ACM, 2017). https://doi.org/10.1145/3025453.3025487.
11. Kyung, G. & Nussbaum, M. A. Driver sitting comfort and discomfort (part II): relationships with and prediction from interface pressure. *Int. J. Ind. Ergon.* **38**, 526–538 (2008).
12. Daynes, S. & Weaver, P. M. Review of shape-morphing automobile structures: concepts and outlook. *Proc. Inst. Mech. Eng. Part D J. Automob. Eng.* **227**, 1603–1622 (2013).
13. Ren, L. et al. Biology and bioinspiration of soft robotics: actuation, sensing, and system integration. *iScience* **24**, 103075 (2021).
14. Mirzaali, M. J., Janbaz, S., Strano, M., Vergani, L. & Zadpoor, A. A. Shape-matching soft mechanical metamaterials. *Sci. Rep.* **8**, 965 (2018).
15. Li, Y. & Yin, J. Metamorphosis of three-dimensional kirigami-inspired reconfigurable and reprogrammable architected matter. *Mater. Today Phys.* **21**, 100511 (2021).
16. Liu, Y., Genzer, J. & Dickey, M. D. "2D or not 2D": shape-programming polymer sheets. *Prog. Polym. Sci.* **52**, 79–106 (2016).
17. Ou, J. et al. Kinetix - designing auxetic-inspired deformable material structures. *Comput. Graph.* **75**, 72–81 (2018).
18. Leeflang, S., Janbaz, S. & Zadpoor, A. A. Metallic clay. *Addit. Manuf.* **28**, 528–534 (2019).
19. Hojjat, M., Stavropoulou, E. & Bletzinger, K.-U. The vertex morphing method for node-based shape optimization. *Comput. Methods Appl. Mech. Eng.* **268**, 494–513 (2014).
20. Ertl, F.-J., Dhondt, G. & Bletzinger, K.-U. Vertex assigned morphing for parameter free shape optimization of 3-dimensional solid structures. *Comput. Methods Appl. Mech. Eng.* **353**, 86–106 (2019).
21. Vu-Bac, N. et al. A NURBS-based inverse analysis of thermal expansion induced morphing of thin shells. *Comput. Methods Appl. Mech. Eng.* **350**, 480–510 (2019).
22. Vu-Bac, N., Rabczuk, T., Park, H., Fu, X. & Zhuang, X. A NURBS-based inverse analysis of swelling induced morphing of thin stimuli-responsive polymer gels. *Comput. Methods Appl. Mech. Eng.* **397**, 115049 (2022).
23. Gosselin, C. M. & Gagnon-Lachance, D. Expandable polyhedral mechanisms based on polygonal one-degree-of-freedom faces. *Proc. Inst. Mech. Eng. Part C J. Mech. Eng. Sci.* **220**, 1011–1018 (2006).
24. Tachi, T. Simulation of rigid origami. In *Origami4: Fourth International Meeting of Origami Science, Mathematics, and Education* 175–187 (A K Peters, Ltd., 2009).
25. Kiper, G. & Söylemez, E. Homothetic Jitterbug-like linkages. *Mech. Mach. Theory* **51**, 145–158 (2012).
26. Thomaszewski, B. et al. Computational design of linkage-based characters. *ACM Trans. Graph.* **33**, 1–9 (2014).
27. Li, R., Yao, Y.-a & Kong, X. Reconfigurable deployable polyhedral mechanism based on extended parallelogram mechanism. *Mech. Mach. Theory* **116**, 467–480 (2017).
28. Hu, Y. & Liang, H. Folding simulation of rigid origami with Lagrange multiplier method. *Int. J. Solids Struct.* **202**, 552–561 (2020).
29. Gao, Y., Wei, X., Han, X., Zhou, Z. & Xiong, J. Novel 3D auxetic lattice structures developed based on the rotating rigid mechanism. *Int. J. Solids Struct.* **233**, 111232 (2021).
30. Besl, P. & McKay, N. D. A method for registration of 3-D shapes. *IEEE Trans. Pattern Anal. Mach. Intell.* **14**, 239–256 (1992).
31. Veltkamp, R. Shape matching: similarity measures and algorithms. In *Proceedings International Conference on Shape Modeling and Applications* 188–197 (IEEE Computer Society, 2001). http://ieeexplore.ieee.org/document/923389/
32. Belongie, S., Malik, J. & Puzicha, J. Shape matching and object recognition using shape contexts. *IEEE Trans. Pattern Anal. Mach. Intell.* **24**, 509–522 (2002).
33. García de Jalón, J., Unda, J., Avello, A. & Jiménez, J. M. Dynamic analysis of three-dimensional mechanisms in "natural" coordinates. *J. Mech. Transm. Autom. Des.* **109**, 460–465 (1987).
34. Nikravesh, P. E. & Affifi, H. A. Construction of the equations of motion for multibody dynamics using point and joint coordinates. In *Computer-Aided Analysis of Rigid and Flexible Mechanical Systems* (eds. Seabra Pereira, M. F. O. & Ambrósio, J. A. C.) 31–60 (Springer Netherlands, 1994). https://doi.org/10.1007/978-94-011-1166-9_2.
35. García de Jalón, J. & Bayo, E. *Kinematic and Dynamic Simulation of Multibody Systems: The Real-Time Challenge*. Mechanical Engineering Series (Springer New York, 1994). https://doi.org/10.1007/978-1-4612-2600-0.
36. Attia, H. A. Dynamic modelling of planar mechanisms using point coordinates. *KSME Int. J.* **17**, 1977–1985 (2003).
37. Nikravesh, P. E. An overview of several formulations for multibody dynamics. In *Product Engineering* (eds. Talabă, D. & Roche, T.) 189–226 (Kluwer Academic Publishers, 2005). https://doi.org/10.1007/1-4020-2933-0_13.
38. Melanz, D., Fang, L., Jayakumar, P. & Negrut, D. A comparison of numerical methods for solving multibody dynamics problems with frictional contact modeled via differential variational inequalities. *Comput. Methods Appl. Mech. Eng.* **320**, 668–693 (2017).
39. Gay Neto, A. Framework for automatic contact detection in a multibody system. *Comput. Methods Appl. Mech. Eng.* **403**, 115703 (2023).
40. Shaw, L. A. & Hopkins, J. B. An actively controlled shape-morphing compliant microarchitectured material. *J. Mech. Robot.* **8**, 021019–1–021019–10 (2015).
41. Huttenlocher, D., Klanderman, G. & Rucklidge, W. Comparing images using the Hausdorff distance. *IEEE Trans. Pattern Anal. Mach. Intell.* **15**, 850–863 (1993).
42. Schwab, A. L. & Meijaard, J. P. How to draw Euler angles and utilize Euler parameters. In *Volume 2: 30th Annual Mechanisms and Robotics Conference, Parts A and B* 259–265 (ASMEDC, 2006). https://asmedigitalcollection.asme.org/IDETC-CIE/proceedings/IDETC-CIE2006/42568/259/318134.

Acknowledgements

This work is part of the research program: "Metallic clay: shape-matching orthopedic implants" with project number 16582, which is financed by the Dutch Research Council (NWO), The Netherlands. P.H.dJ. would like to thank Judith Cueto Fernandez for the support in the early stage shaping of the text and the virtual sculpting of the undefined 3D "blend" (Fig. 2c).

Author contributions

P.H.dJ. and A.A.Z. conceived the study. A.L.S. formulated the model. P.H.dJ. and M.J.M. designed the experiments. P.H.dJ. performed both the simulations and experiments. P.H.dJ., M.J.M., and A.A.Z. contributed to data interpretation. A.L.S., M.J.M., and A.A.Z. supervised the study. A.A.Z. obtained funding for the study. P.H.dJ. wrote the first draft of the manuscript. All authors edited the manuscript for actual intellectual content and approved the final manuscript.

Competing interests

A.A.Z. is a Guest Editor for Communications Materials and was not involved in the editorial review of, or the decision to publish, this Article. All other authors declare no competing interests.

Additional information

Supplementary information The online version contains supplementary material available at https://doi.org/10.1038/s43246-023-00410-2.

Correspondence and requests for materials should be addressed to Pier H. de Jong or Mohammad J. Mirzaali.

Peer review information *Communications Materials* thanks Tino Stankovic and the other, anonymous, reviewer(s) for their contribution to the peer review of this work. Primary Handling Editor: Aldo Isidori. A peer review file is available.